bcc-to-hcp transformation pathways for iron versus hydrostatic pressure: Coupled shuffle and shear modes

J. B. Liu and D. D. Johnson
Department of Materials Science and Engineering, University of Illinois at Urbana-Champaign, Urbana, Illinois 61801, USA
(Received 22 October 2008; revised manuscript received 16 March 2009; published 22 April 2009)

Using density-functional theory, we calculate the potential-energy surface (PES), minimum-energy pathway (MEP), and transition state (TS) versus hydrostatic pressure σ_{hyd} for the reconstructive transformation in Fe from body-centered cubic (bcc) to hexagonal closed-packed (hcp). At fixed σ_{hyd}, the PES is described by coupled shear (ϵ) and shuffle (η) modes and is determined from structurally minimized hcp-bcc energy differences at a set of (η,ϵ). We fit the PES using symmetry-adapted polynomials, permitting the MEP to be found analytically. The MEP is continuous and fully explains the transformation and its associated magnetization and volume discontinuity at TS. We show that σ_{hyd} (while not able to induce shear) dramatically alters the MEP to drive reconstruction by a shuffle-only mode at $\leq$30 GPa, as observed. Finally, we relate our polynomial-based results to Landau and nudge-elastic-band approaches and show they yield incorrect MEP in general.

DOI: 10.1103/PhysRevB.79.134113 PACS number(s): 64.70.kd, 05.70.Fh

There is a long history in the study of reconstructive transformations in iron due to its importance in understanding of technological Fe-based materials and geophysical phenomena, which are highly dependent upon our knowledge of the pressure, shear, and temperature phase stability of iron and its alloys.[1] Iron bcc is the low-pressure ground state, while under σ_{hyd} loading from 9 to 25 GPa hcp iron becomes stable with a magnetization and volume collapse at the transition.[2–12] Theoretical attempts have been made to understand this key bcc-to-hcp reconstructive transformation and its associated properties, including pressure dependence, with estimates for the transition pressure from 50 to 200 GPa.[13–18] Stability at extreme pressures and temperatures have been studied, too.[19–21] However, no one has determined the fixed-pressure potential-energy surface (PES), minimum-energy path (MEP), transition state (TS), and the associated discontinuities, especially versus increasing σ_{hyd}.

It is generally accepted that bcc-hcp reconstructive transformation follows the so-called Burgers mechanism,[22] in which the crystal undergoes simultaneous shear deformation with alternating shuffle of the adjacent atomic planes [see Fig. 1] described as

$$(110)_{bcc} \| (0001)_{hcp} \text{ and } [\bar{1}11]_{bcc} \| [\bar{2}110]_{hcp}. \quad (1)$$

Two coupled steps are needed, namely: (1) a strain $\epsilon\{001\}\langle 001\rangle$ along $[001]_{bcc}$ reducing the angle θ_c from 70.53° to 60° between the two $(110)_{bcc}$ diagonals to make perfect hexagons; and (2) an internal shear strain $\eta\{110\}\langle 1\bar{1}0\rangle$ along $[\bar{1}10]_{bcc}$ shuffling atoms in every second layer into the hcp positions. It is often assumed for simplicity that these two steps are decoupled and sequential, often (improperly) called Burger's path. In reality, these two steps must happen simultaneously; see Fig. 2.

However, hydrostatic pressure alone cannot produce shear, only deviatoric stress can (i.e., $\Delta\sigma=\sigma-\sigma_{hyd}$, where σ is symmetric stress and σ_{hyd}=Trace $\sigma/3$). So, generally, the shear-induced bcc-hcp transformation can have the MEP and TS altered dramatically by pressure. For example, if pressure could move the TS to a pure-shuffle mode, the bcc N-point phonon could drive the system to the TS, and the shear would be completed downhill in energy. This general picture of the transformation and its pressure dependence, addressed here, has not been studied before. Such a pathway is the antithesis of the decoupled and sequential path often assumed.

By way of background, we highlight some of the key theory papers addressing bcc-hcp transformation. Both linear muffin-tin orbital (LMTO) method,[13] and full-potential linearized-augmented plane-wave (FLAPW) method[14,18] have been used to study the energetics of bcc, fcc, and hcp structures in iron at high pressure within density-functional theory (DFT) via a generalized gradient approximation (GGA) for electron exchange correlation. Fe bcc was found to be mechanically unstable at high pressure (100 GPa), but no details (MEP nor TS) of the bcc-hcp transformation were determined. Ekman *et al.*[16] investigated extensively the bcc-hcp transformation in iron using FLAPW-GGA. They presented *fixed-volume* PES plots of the total energy as a func-

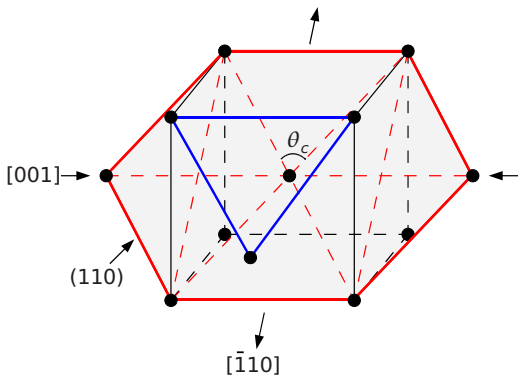

FIG. 1. (Color online) Coupled shuffle and shear (η,ϵ) required for bcc-to-hcp transformation. Shaded bcc (110) requires compression (and/or dilation) along [001] ($[\bar{1}10]$) to form hexagons. Atoms in adjacent {110} (connected by blue lines) require a shuffle to create hcp stacking; see Fig. 2.

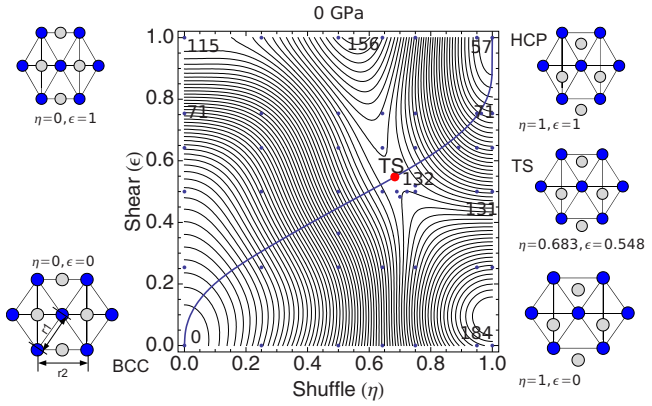

FIG. 2. (Color online) PES contours from $F(\eta,\epsilon)$ via DFT data (dots), MEP (solid curve), and TS of 132 meV/atom (red circle). PES values (in meV) at (η,ϵ) are from $F(\eta,\epsilon)$. Atom projections in (110) planes are shown at various (η,ϵ).

tion of shear and shuffle, so continuous volume relaxations versus fixed (η,ϵ) were not allowed; instead, several volumes were chosen in order to simplify the calculations. Studying enthalpies at fixed smaller volumes (i.e., higher pressures) they suggested that room-temperature phonon excitation might enable a transition at 50 GPa. Experimental data[4,12] suggest that there is a non-negligible (8–10 %) abrupt volume decrease along the bcc-to-hcp transformation path, and that the transformation starts and completes from 13.8–16.2 GPa (Ref. 12) (formerly[4] 9–22 GPa), with hysteresis upon unloading.

Recently, a *solid* nudge-elastic band (NEB) method was proposed[23] that sets the shear (unit cell) modes continuously and permits the shuffle (internal cell) mode to follow the minimum in the force, in distinction to standard nudge-elastic band[24] in which atomic motions are continuous, as required physically. Using this approach, Johnson and Carter[25] investigated the PES and MEP in Fe and found a discontinuous jump in atomic shuffle degrees of freedom giving a very low bcc-to-hcp barrier. (Such jumps, however, are unphysical, and a consequence of the method, see Sec. III.) Lindgard and Mouritsen[26] and Sanati *et al.*[27] studied the hcp-to-bcc (temperature phonon-induced) reconstructions in Ti and Zr, employing an approximate Landau free-energy approach based on DFT energies. While presented as a general, their approach was not used for the Fe bcc-to-hcp transformation. We show that both the Landau and NEB methods produce the same discontinuous (and unphysical) MEP that follows the initial eigenvectors at the minima (bcc or hcp) but lead to a discontinuous (and unphysical) atomic motion with artificially low barriers from ignoring the large coupling between shuffle and shear modes.

Here, we demonstrate a direct method to obtain the MEP in the bcc-hcp reconstructive transformation. The method, however, is applicable to any general transformation involving coupled modes. Using a large set of DFT hcp-bcc energy differences at fixed pressures (0, 10.5, and 22 GPa), we apply the method to the phase transition in Fe from the ferromagnetic (FM) bcc to the nonmagnetic (NM) hcp yielding results all in agreement with observed effects at the transition state. As a function of $\sigma_{\rm hyd}$, we determine the global PES, continuous MEP, and the TS, and fully explaining observed the bcc-hcp transformation and associated magnetization and volume discontinuities at TS.[2–4,7,10–12] We show that the magnetization collapse is not generally due to $\sigma_{\rm hyd}$, but simply inherent to the behavior of Fe during the shuffle-shear transformation. Versus $\sigma_{\rm hyd}$ we show that the PES and TS are altered in such a way to permit a pure-shuffle mode at $\leq$30 GPa to drive the system to TS, in agreement with observation.[4,12] [We find competing spin states after crossing the TS into the hcp basin, but the lowest at given (η,ϵ) is nonmagnetic. At perfect hcp $(\eta\rightarrow 1,\ \epsilon\rightarrow 1)$, antiferromagnetic order[18] or fluctuations[28] may be relevant and only slightly affect our results.] Our results provide a better understanding of Fe-based materials transformation and related pressure experiments.

I. METHODS DETAILS

In order to determine the bcc-hcp MEP, we require accurate structural-energy differences $\Delta E(\eta,\epsilon)$ between bcc $(\eta=0,\ \epsilon=0)$ and any distorted state (η,ϵ), including ideal hcp $(\eta=1,\ \epsilon=1)$; see Fig. 2. We use spin-polarized, *ab initio* DFT calculations to describe properly the magnetization and to obtain a large set of total-energy difference $\Delta E(\eta,\epsilon)$ relative to bcc. To obtain the PES in reasonable computational time and provide a general approach, we use a symmetry-adapted "free-energy" polynomial to provide an analytic determination of the TS and the MEP by fitting to a finite set of DFT results, with more sets are around TS due to higher curvature. $\Delta E(\eta,\epsilon)$ was obtained by minimizing the total energy versus volume (V in Å^3) and magnetization (μ in μ_B) for fixed ($\sim$45) values of (η,ϵ) and $\sigma_{\rm hyd}$. We stress that this is a generic approach to obtain the MEP analytically via an accurate polynomial representation that reflects all symmetry requirements for solid-solid transformation.

DFT Method. We use a pseudopotential plane-wave method, as implemented in the Vienna *ab initio* simulation package (VASP),[29,30] that uses the projector augmented wave (PAW) basis[31] to yield accurate energy differences. The exchange-correlation functional is a nonlocal GGA.[32] The VASP-PAW-GGA approaches the all-electron FLAPW method, and it correctly predicts the ordering of structural and magnetic states of Fe. We use 350 eV energy cutoff for the plane-wave basis set and a $20\times20\times20$ Monkhorst-Pack[33] mesh for Brillouin-zone integrations. Convergence of the total energies (forces) is less than 4 meV/atom (2 meV/Å).

PES Determination. To describe well the entire PES within a limited set of DFT energy differences and determine the MEP analytically, we fit our $\Delta E(\eta,\epsilon)$ data to a symmetry-adapted polynomial that properly represents the PES. For this strain-energy functional $F(\eta,\epsilon)$, we choose a fourth-order cosine and sine polynomial, i.e.,

$$F(\eta,\epsilon)=\sum_{m,n=0}^{m+n\leq 4} a_{mn}[X(\eta)]^m[X(\epsilon)]^n[1-\delta_{m0}\delta_{n0}] + \sum_{m,n=1}^{m+n\leq 4} b_{mn}[X(\eta)]^m[Y(\epsilon)]^n, \quad (2)$$

with $X(x)=[1-\cos(\pi x)]$ and $Y(x)=\sin(\pi x)$, and b_{0n} and b_{m0}

terms represented by a_{mn}. Form (2) of the strain-energy function satisfies all boundary conditions and symmetries. First, $F(0,0)$ must be zero because bcc is the reference state; so $a_{00}=b_{00}=0$ and these terms are excluded in Eq. (2) by Kronecker's deltas [δ_{ij} is 1(0) if i is (not) equal to j]. Second, $F(\eta,\epsilon)$ must be symmetric to shuffle η, i.e., $F(\eta,\epsilon)=F(-\eta,\epsilon)$, as shuffle by η along $[1\bar{1}0]_{\rm bcc}$ or $[\bar{1}10]_{\rm bcc}$ in (110) is same structure. However, $F(\eta,\epsilon)$ is not symmetric to shear ϵ, i.e., $F(\eta,\epsilon)\neq F(\eta,-\epsilon)$, as moving atoms closer costs more energy; see Fig. 1. Third, to ensure (meta-) stable structures, as found in the DFT, are properly described, $F(\eta,\epsilon)$ should have local minima at (0,0) and at (1,1), i.e., the constraints are

$$\left.\frac{\partial F}{\partial x}\right|_{x=0,1}=0, \tag{3}$$

where $x=\{\eta,\epsilon\}$, which is satisfied by Eq. (2). In the fitting of $F(\eta,\epsilon)$, we should also use a minimal number of coefficients so as not to over fit to the DFT results. We find for Fe that the coefficients b_{13} and b_{31} are negligible, and we neglect these in results presented below.

Notably, the X and Y functions inherently contain terms of $\eta^m\epsilon^n$ in Taylor's series, permitting connection to Landau approaches and their corresponding MEP analysis, while keeping form as simple as possible for analytic determination of the correct MEP. The sums in $F(\eta,\epsilon)$ are restricted to $m+n\leq 4$ to satisfy all constraints and match a Landau theory when Taylor's series expanded. As such, the strain-energy functional in Eq. (2) can be considered a Landau-type free-energy functional for the reconstructive bcc-to-hcp transformation in terms of coupled shuffle and shear modes. We will use this to discuss common Landau approaches to determine the MEP. While the fit coefficients a_{mn} and b_{mn} generally describe the topology of the PES, they also can provide the physical coupling parameters and Landau coefficients, as seen after expanding by equating to coefficients in Sec. III.

MEP Determination. To describe fully the transition, the MEP is required and can be determined directly given $F(\eta,\epsilon)$ fit to DFT energy differences. The MEP is the lowest-energy path connecting two minima on a PES. For a process with only one transition state, the MEP is given by the steepest-descent path from the TS to each minima.[34–36] The TS is the smallest saddle-point energy. Often the only information known when searching for the MEP is the start and end points, normally located at the PES minima. If the TS is located, the MEP can be efficiently obtained by following the gradient of the energy downhill, along the eigenvectors leading to the two minima. Having fit our DFT results to the symmetry-adapted polynomial in Eq. (2) we determine the energy-gradient $\nabla F(\eta,\epsilon)$ analytically; we then find the TS as the saddle-point $(\eta_{\rm TS},\epsilon_{\rm TS})$ having the smallest maximum magnitude of $F(\eta,\epsilon)$; then, starting from TS, we follow the eigenvectors of $F(\eta_{\rm TS},\epsilon_{\rm TS})$, found analytically, downhill to each minimum, yielding the MEP. Functionally, we numerically obtain the MEP from the strain-energy function using the analytic gradient in three steps: (a) move a small step along the gradient direction (local eigenvector) toward one minima; (b) calculate the gradient at the new position; (c) repeat steps (a) and (b) until we reach bcc or hcp state.[34,35] Both the fitting to DFT results to get the PES, as well as the analytic determination of the MEP are handled using MATHEMATICA.[37]

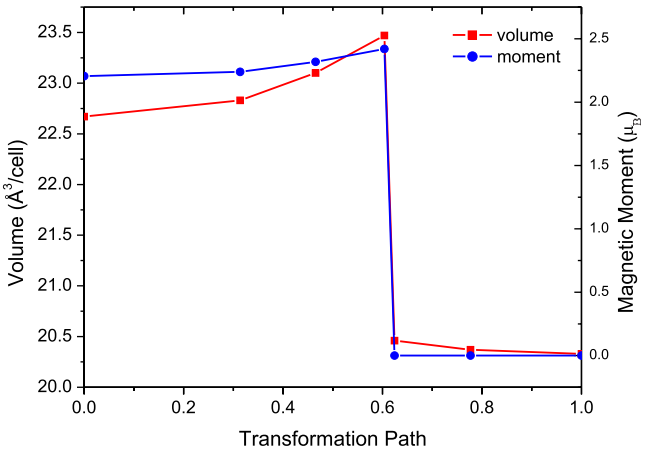

FIG. 3. (Color online) Calculated Fe volume (in Å^3, squares) and magnetic moments (in μ_B/atom, circles) along the 0 GPa MEP. At the TS in Fig. 2, a first-order moment collapse occurs (from $2.42\mu_B$) with concomitant volume discontinuity.

Importantly, one *does not find* the correct MEP by minimizing the strain-energy function serially with respect to the shear (or shuffle) order parameter, as done in Landau approach,[26,27] because the η and ϵ modes are strongly coupled and not independent modes. Due to this the Landau functional and nudge-elastic band methods yield the wrong MEP, as discussed in Sec. III.

II. RESULTS FOR BCC-TO-HCP MEP

In Fig. 2 we show a PES contour plot for Fe bcc-to-hcp obtained from the symmetry-adapted polynomial (strain-energy values) $F(\eta,\epsilon)$ fit to DFT $\Delta E(\eta,\epsilon)$ data at 0 GPa. Later, energy values from the strain-energy $F(\eta,\epsilon)$ are important for comparison to Landau or nudge-elastic-band results. For specific (η,ϵ), we show the projections of the atoms in adjacent (110) planes. The actual (η,ϵ) where the DFT $\Delta E(\eta,\epsilon)$ was obtained is also indicated in Fig. 2; specific values of the PES (in meV), magnetic moments (in μ_B/atom) and volumes (in Å^3/cell) for given states at 0, 10.5 and 22 GPa are listed in Tables I–III, respectively, in the Appendix. The associated magnetism and volume change at the TS along the MEP at 0 GPa is given in Fig. 3. Figure 4 shows comparative results for 10.5 and 22 GPa, near the calculated and observed start and end pressures for the transformation. From these results we estimate a shuffle-only transition at $\leq$30 GPa, which can be pure phonon driven. These results constitute the first complete and quantitative calculation of the global PES, MEP, and TS for the bcc-to-hcp transformation that include full volume relaxation and magnetization effects for all shuffle-shear modes at fixed, hydrostatic pressures.

From Fig. 2, the energy barrier at 0 GPa for the MEP is 132 meV/atom at the TS, similar to the 122 meV/atom found using constrained-volume calculations.[16] One can visually

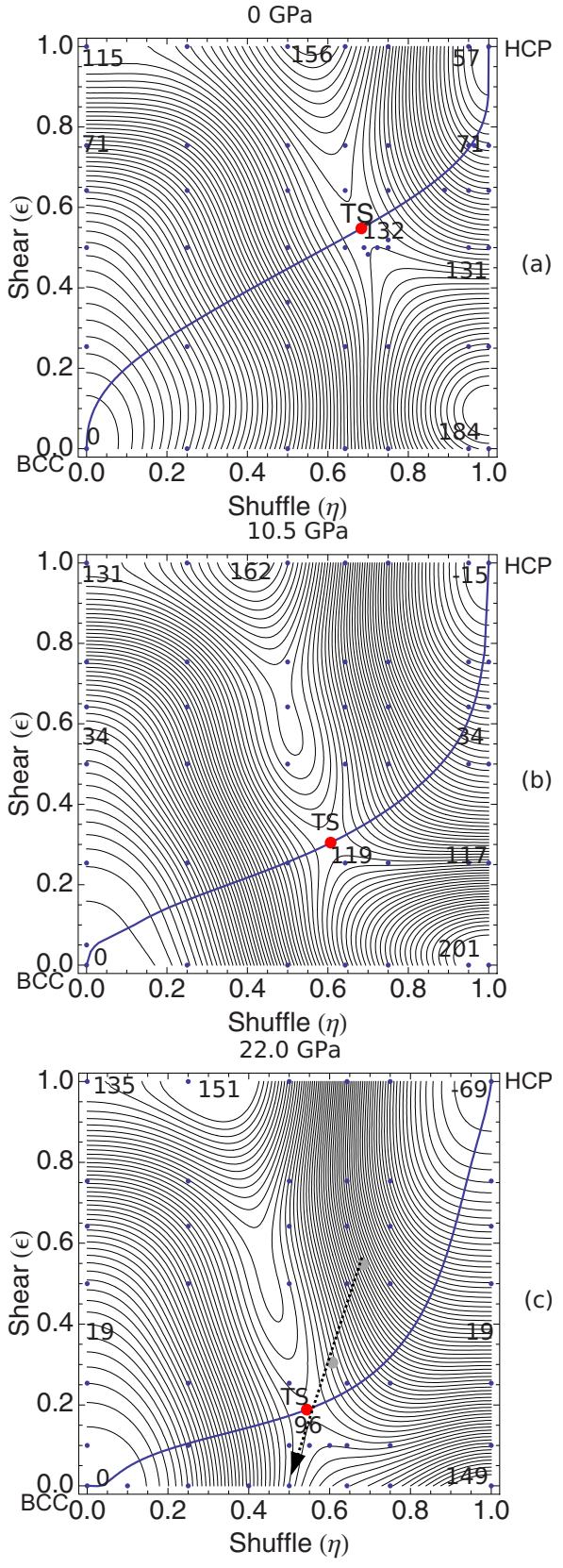

FIG. 4. (Color online) Iron PES contours and TS (red dots) at (a) 0; (b) 10.5; and (c) 22 GPa. Blue dots given location of DFT results. Gray dots in (c) are the TS for 0 and 10.5 GPa, and dashed arrow shows trend of TS to pure shuffle (η=0.5 and ϵ=0) at pressure of $\leq$30 GPa.

confirm [from the MEP at (0,0)] that the initial eigenvector upon starting the transformation at bcc lies along $(\eta=0,\epsilon)$, where the energy per strain is lowest, i.e., larger separation between contour lines. Starting at bcc, the journey along zero-shuffle mode $(\eta=0,\epsilon)$ remains quite low in energy up to large shears, albeit this is not the MEP. This zero-shuffle mode is along the sequential Burger path, i.e., $(0,\epsilon)\rightarrow(0,1)\rightarrow(1,1)$, with 156 meV/atom barrier at $(\eta=0.4,\ \epsilon=1)$ to the hcp state. Similarly, starting at hcp, the eigenvector points along a path given by the low-energy, zero-(reverse)shuffle mode point along $(\eta=1,\epsilon)$. The true MEP, which remains perpendicular to the gradient of the PES obtained via the gradients of $F(\eta,\epsilon)$, connects these initial eigenvectors to form a path through the TS having the lowest saddle-point energy.

A signature of the transformation under pressure is a volume collapse observed at the TS.[2–4,7,10–12] Figure 3 shows the calculated magnetism and volume change along the bcc-to-hcp MEP at 0 GPa. (The region of zero magnetization, on the hcp side of the saddle point, is evident from result listed in Tables I–III in the Appendix.) We emphasize that the results in Fig. 3 are for 0 GPa, although similar results hold at all pressures (not shown), indicating that these effects along the MEP are generic to Fe, and occur due to shuffle-shear rather than specifically pressure. Indeed, just before the TS, the magnetic moment on each atom is close to that of bcc Fe, and the cell volume increases slightly from 22.67 (bcc) to 23.47 Å^3/cell/cell (TS), a 3.5% increase. Passing through the TS, the moments collapse from $2.42\mu_B$/atom to $0\mu_B$/atom and the volume drops discontinuously from 23.47 to 20.33 Å^3/cell, a −13.4% drop. The collapse of magnetism drives the volume change. Again, a result of the hcp-like structural change after TS, rather than pressure-induced volume reduction, like those addressed in former DFT calculations.

We emphasize that even though all atoms move continuously, as is physically required [see Fig. 2 insets of the structures] both the volume and magnetism exhibit a correlated discontinuity at TS. The magnetic moment collapse, a feature of a first-order phase transition, is in agreement with the similar drop found previously.[13,15,16] In addition, Ekman *et al.*[16] described a cusp in the phonon spectra in their fixed-volume calculations. This cusp arises at the TS due to the volume discontinuity in the free-energy functional, which is reflected in the phonon spectra (phonons being related to the second derivatives of free energy). Note that atomic coordinates are always continuous degrees of freedom even though collective behavior, such as phonons, and nonconserving integral quantities, such as volume and magnetization, can exhibit discontinuities in first-order phase changes. As a result, the MEP will be continuous because it depends on all the atomic (continuous) degrees of freedom. These comments will have critical relevance to erroneous results that will be obtained from Landau and nudged-elastic band methods; see Sec. III.

Under pressure the thermodynamically stable phase is given by minimizing the enthalpy, $H=E+PV$. We find that bcc and hcp are degenerate at ~9.5 GPa, near the reported onset σ_{hyd} for the transformation. However, only the deviatoric stress can induce shear in a solid, so σ_{hyd} is not solely

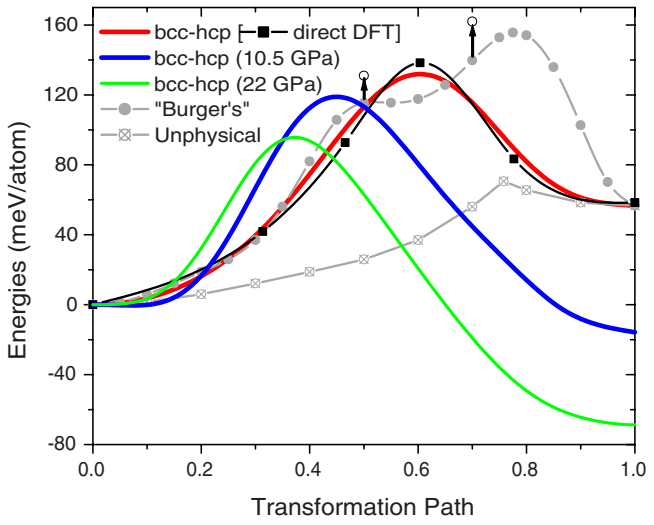

FIG. 5. (Color online) Paths from $F(\eta,\epsilon)$: MEP (red 0, blue 10.5, and green 22 GPa), serial Burger's (gray circles), and unphysical solid NEB (gray squares). DFT values (black squares) along MEP to show the goodness of the fit. Vertical arrows mark the change in energy at 10.5 GPa along the serial Burger's path, while hcp drops 75 meV relative to 0 GPa.

responsible for the shuffle-shear transformation, which can happen also at 0 GPa; see Fig. 2. Above 10 GPa four major pressure effects are evident; see Fig. 4: (1) the TS is now globally the lowest bcc-to-hcp barrier, so the lowest pathway (and eigenvector) is directly up hill to the saddle point (TS); (2) the hcp energy drops (relative to bcc) from 57 meV/atom at 0 GPa to −15 meV/atom at 10.5 GPa, and to −69 meV/atom at 22 GPa; and, once hcp, (3) the hcp structure remains more stable with respect to pressure. Thus, bcc becomes energetically metastable relative to hcp above 10.5 GPa, in agreement with previous work.[15–17] And, finally, (4) increasing $\sigma_{\rm hyd}$ further [see Fig. 4(c) at 22 GPa] moves TS toward (η,ϵ) of (0.5, 0), permitting a pure-shuffle (zero strain) mode to achieve the transition. For 22 GPa a smaller energy barrier of 96 meV (40% smaller barrier than that found previously[16]) is required. We estimate $\lesssim$30 GPa (much less that the 50–200 GPa from fixed-volume results[13–17]) is needed to reach the bcc-hcp TS by a N-point phonon at room temperature. A phonon-mediated transition was suggested by Ekman *et al.*[16]

In Fig. 5, we compared the calculated energy versus transformation path (the MEP) under pressure to the serial "Burger's path," as well as the (unphysical) nudged-elastic band or Landau free-energy path discussed later. At 10.5 GPa, there is still an energy barrier between bcc and hcp, i.e., ΔE is 119 meV/atom versus 132 meV/atom at 0 GPa, a decrease of ~10%. Hence, with hcp lower in energy than bcc above 10 GPa, the presence of the asymmetric barrier between them gives rise to small hysteresis under cycling of pressure through the transition, as is observed.[4,12] This hysteresis is due to kinetics and thermal excitations under pressure as the system is exploring phase space to complete the transformation, which controls the percentage of hcp appearing in the sample. The energy barriers from Fig. 4 can be used to estimate the range of transformation pressure by $\Delta P \approx \Delta E/(V_{\rm bcc}-V_{\rm hcp})$ with volumes of 22.67 Å^3 (bcc) and 20.33 Å^3 (hcp); see Fig. 3. A barrier of 132 meV/atom (184 meV/atom) at 0 GP leads to a minimum (maximum) onset transformation pressure of 9 GPa (12.6 GPa). At 10.5 GPa, the minimum (maximum) barrier is 119 meV/atom (201 meV/atom), giving pressure of 8.1 Gpa (13.8 GPa). At 22 GPa, the minimum (maximum) barrier is 96 meV/atom (149 meV/atom), giving pressure of 6.6 GPa (10.2 GPa). At 22 GPa, the pathway dependent hysteresis is 3.6 GPa, close to latest observed value.[12]

III. RELATION TO LANDAU AND NUDGE-ELASTIC BAND METHODS

For completeness, we discuss how Landau free-energy (LFE) expansion and solid-NEB approaches can yield the incorrect MEP for reconstructive transformations. Recall, the symmetry-adapted free-energy polynomial in Eq. (2) permits a direct comparison to Landau-type polynomial functional used in previous works, which will also be related to the nudge-elastic band results. Keep in mind that the PES is multivalued in (η,ϵ), as clear from Figs. 2 and 4, which lead to bifurcation points in the solutions of MEP, if not performed globally. Indeed, as we now show, standard solutions via LFE or NEB methods can lead to unphysical discontinuities as a result.

The temperature-dependent, reconstructive hcp-to-bcc transformation, as observed in Ti and Zr, for example, has been described by Lindgard and Mouritsen[26] (LM) and Sanati *et al.*[27] in terms of LFE with respect to shuffle η and shear ϵ order parameters, too. Using symmetry and a polynomial that assumes the order parameters are small, the LFE is

$$F(\eta,\epsilon)=\frac{A}{2}\eta^2+\frac{B}{4}\eta^4+\frac{C}{6}\eta^6+\frac{A_1}{2}\epsilon^2+\frac{B_1}{4}\epsilon^4+C_1\epsilon\eta^2, \quad (4)$$

where the C_1 term couples the external shear with internal shuffle. Sanati *et al.*[27] added higher-order coupling terms to Eq. (4), while ignoring terms higher order than ϵ^2 to improve the fit between the LFE and DFT calculations. Their functional form does improve the fit, but not the qualitative results. Thus, we focus on the simple form in Eq. (4). Note that a sixth-order polynomial in shuffle is required to describe a first-order transformation.

Given Eq. (4) a fit to any DFT data can be made to get the coefficients in $F(\eta,\epsilon)$. For these coefficients, $F(\eta,\epsilon)$ is minimized with respect to strain (ϵ) at fixed shuffle (η), i.e., $\partial F_{\rm LM}/\partial\epsilon|_\eta=0$, to obtain $\epsilon[\eta]\approx-\frac{C_1}{A_1}\eta^2$. By substituting into (4), we find a simple one-parameter free-energy $F(\eta,\epsilon[\eta])$ defining the *apparent* MEP, i.e.,

$$F^{\rm MEP}(\eta)\approx\frac{A}{2}\eta^2+\frac{[B-2C_1^2/A_1]}{4}\eta^4+\frac{C}{6}\eta^6. \quad (5)$$

This MEP depends not only upon the assumed coupling but

also the size and specific order of truncation. Also, the solution of this equation leads to bifurcation points (imaginary solutions) that lead to discontinuities in the MEP, as found also for NEB recently.[25] We now reproduce such results from our PES, as shown in Fig. 5 with a cusplike MEP with small, but incorrect, barrier.

For a comparison, we fit the Lindgard-Mouritsen and Sanati *et al.* forms to our DFT results for Fe bcc-to-hcp transformation, and compared them to our generic formulation in Eq. (2). Neither were able to fit the case of Fe well. In particular, they failed to reproduce the local stability of hcp structure (i.e., hcp is not a local minimum of the functional). We can quantify the goodness of each of the three LFE forms by the least-squared fit error.[38] We find at 0 GPa that κ^2 are 112.9, 68.5, and 25.8 for the Lindgard-Mouritsen, Sanati *et al.*, and our polynomials, respectively. Our Eq. (2) provides a much better fit to the first-principles data mainly due to the fact that we are not trying to approximate a LFE just trying to fit the PES more accurately based upon symmetry requirements; then, due to its (co)sine form, we can, if we wish, make an analytic connection to any LFE forms.

We can now follow the approach outlined above for finding the MEP with our LFE; that is, we minimize Eq. (2) analytically with respect to strain to obtain an effective one-dimensional LFE in terms of only shuffle, then numerical solve for the MEP. Starting at bcc, the numerical solution of the resulting MEP equation following this approach yields a MEP along (η=0, ϵ=0) to (η=0, ϵ=0.75) with a discrete (and hence, instantaneous in time) jump in shuffle (a bifurcation point in this approximate solution) to (η=1, ϵ=0.75) and ends downhill at hcp. Values of the strain energy along this MEP are marked in Fig. 2 where the energies at (η=0, ϵ=0.75) and (η=1, ϵ=0.75) are both 71 meV/atom. Therefore, 71 meV/atom is the "barrier at the TS" at 75% along the "unphysical" MEP in Fig. 5, which appears as a cusp. The pathway is unphysical due to the assumption that the MEP is determined by uncoupling the shear and shuffle degrees of freedom (during the minimization versus shear) and then matching free-energy values. The MEP obtain by Eq. (5) also yields a similar result, as it must.

Importantly, however, the apparent MEP determined in this way is not the correct MEP if the modes are highly coupled. For general reconstructive phase transitions the order parameters are not the simple shuffle and shear but transcendental order parameters.[39] Hence, the PES is multivalued in the intuitive shuffle and shear order parameters (legitimately written down for reconstruction). Hence, the simple minimization procedure fails to yield the MEP. One finds the MEP and TS using the standard technique noted in Sec. I, i.e., follow the gradient from the TS to each minima (solid curves in Figs. 4 and 5).

All this can be seen directly in the PES. In Fig. 2, one can visually confirm that the initial eigenvector upon starting the transformation at bcc lies along (η=0,ϵ) where the energy per strain is lowest [the correct MEP shows the starting eigenvector at (0,0)]. If there is no constraint to follow the MEP that remains perpendicular to the gradient of the PES, as necessary in any transformation, then indeed the lowest-energy (fictitious) path is along the zero-shuffle mode. Starting at bcc, the zero-shuffle mode is the beginning of the often assumed serial Burger's path, leading to a TS at 156 meV/atom at (η=0.6, ϵ=1) before reaching the hcp state, which is higher than the 132 meV/atom at the true TS in Fig. 2.

Starting at bcc, the MEP obtain by (5) must be along η =0, forcing it along the zero-shuffle mode. Similarly, starting at hcp, the lowest-energy (fictitious) path is along the shear mode (η=1, ϵ=1) to (η=1, ϵ=0). Hence, the only way that the transformation path can be connected between the bcc initial eigenvector and hcp initial eigenvector is to assume that the free energies are equal at the transition state, thereby defining the TS (improperly) without gradients. In Fig. 2 only ϵ=0.75 satisfies this assumption, giving $F(\eta=0,\ \epsilon=0.75)=F(\eta=1,\ \epsilon=0.75)$, and a TS at 71 meV/atom, see "unphysical" MEP in Fig. 5. While this is lower than the true TS of 132 meV/atom, it is an improperly defined transition that exhibits an unphysical discontinuous (and instantaneous) jump in all atomic degrees of freedom, from a structure with (η=0, ϵ=0.75) to one with (η=1, ϵ=0.75). The discontinuity is not in any nonconserving integral quantities, such as volume; it is in the atomic degrees of freedom that should be always continuous.

The true MEP (Fig. 5) is determined by following the eigenvectors at TS down to each minima. The PES under pressure yields similar results, only the starting eigenvectors at TS are rotated toward the pure-shuffle (zero strain) axis; see Fig. 4.

A NEB approach will find the same results as the LFE. A solid-state NEB method[23] fixes the cell degrees of freedom (shear) and fully minimizes all internal degrees of freedom (shuffle), so the full, multivalued PES is not explored. Even with an elastic band coupling both η and ϵ, the bands distort (unless constrained strongly) to follow the small energy per strain along initial eigenvectors at (η=0, ϵ=0) and (η=1, ϵ=1), regardless of where the TS is located. Due to the multivalued PES, you then get exactly same result as the LFE approach: a discontinuous (and instantaneous) jump from a structure with (η=0, ϵ=0.75) to one with (η=1, ϵ=0.75) as we show in Fig. 5 (the curve marked "unphysical"), which matches exactly the very recent solid-NEB result for Fe.[25] The cusp arises due to the discontinuity of the atomic motions from η=0 to 1. In the correct MEP, the atomic motions are continuous through the TS, even while the volume and magnetization are discontinuous, as discussed.

For the LFE and standard NEB in which the shuffle η modes are kept continuous and minimization is made with respect to shear ϵ, the MEP is again unphysical and has the wrong curvature, but it at least passes near the correct TS, because the internal shuffle are now continuous (cell shear modes are not).

Thus, neither the Landau nor NEB methods yield the physical MEP for solid-state reconstructions involving on η and ϵ. On the other hand, the symmetry-adapted polynomial permits the MEP to be found analytically following the gradients from the TS to each minima and describes properly the reconstructive transformation, including the all observed discontinuities and hysteresis.

IV. CONCLUSIONS

Using density-functional theory, we have studied the pressure-induced, bcc-to-hcp reconstruction in Fe arising from the coupled internal shuffle (η) and shear (ϵ) degrees of freedom, with full volume relaxations included in the potential-energy surface versus (η, ϵ). To do so, we have provided a reliable method to address solid-solid reconstructive transformations by employing a symmetry-adapted polynomial to obtain the full PES from a fit to DFT structural-energy differences. The polynomial permits the minimum-energy path and its transition state to be found analytically. Moreover, the polynomial allows a direct connection to Landau and nudge-elastic band methods, showing that neither method gets the correct transformation path.

As hydrostatic pressure (σ_{hyd}) cannot produce shear for the transformation to occur, we determined the PES versus σ_{hyd} to understand the transformation and its observed properties. We find that pressure alters the PES and MEP (and its barriers, TS) such that, at $\leq$30 GPa, a pure-shuffle (bcc N-point phonon) mode can reach TS, which is now accessible at even at room temperature. The calculated transition occurs from 10 to 30 GPa, the range in experiment. The MEP is continuous (as are all atomic motions) with a magnetization collapse and concomitant volume discontinuity at the TS, signatures in experiment. Notably, the magnetization and volume collapse are not due specifically to pressure, but to the inherent structural sensitivity of the Fe PES. Taken together these results provide direct insight and explanation for the for the bcc-to-hcp reconstructive transformation in Fe-based materials, including the Earth's core.

ACKNOWLEDGMENTS

Support is from the Department of Energy through Grants No. DEFG02-03ER46026 and No. DEFG36-05GO15045. Work support by National Science Foundation Grants No. DMR 07-05089 and No. DMR-03-13489 has benefited the present work. Computational support from the Materials Computation Center is under Grant No. NSF DMR-03-25939.

APPENDIX

Here we specify the energy, magnetization, and volume values obtained from DFT calculations (identified in Figs. 2 and 4) calculated with full volume relaxation for specific choices of shuffle and shear (η, ϵ) at each hydrostatic pressure. As both η and ϵ parameters are coupled, this is a critical part of the computations. Tables I–III are for 0, 10.5, and 22 GPa, respectively. Various representations of atomic configurations with specific (η, ϵ) pairs are given in Fig. 2. Comparing Figs. 2 and 4 with the values in the tables provides also an idea where the magnetization and volume collapse occurs during transformation to hcp-like symmetry for shuffle and shear parameters not along the MEP given in Fig. 5.

TABLE I. Calculated bcc-to-hcp PES (first row, in meV), magnetic moment (second row, in μ_B/atom) and cell volume (third row, in Å^3/cell) for given shuffle, shear (η, ϵ) at 0 GPa.

ϵ \ η	0.00	0.25	0.50	0.643	0.75	0.95	1.00
	0.00	22.70	76.20	111.10	136.40	179.80	190.40
0.000	2.21	2.22	2.26	2.30	2.31	2.32	2.32
	22.67	22.74	22.98	23.22	23.32	23.48	23.52
	7.50	29.50	81.00	112.90	136.30	172.65	178.10
0.250	2.21	2.23	2.29	2.32	2.34	0.00	0.00
	22.69	22.78	23.05	23.19	23.32	20.60	20.61
	27.75	49.05	97.50	127.00	136.95	115.05	115.25
0.500	2.24	2.26	2.34	2.37	0.00	0.00	0.00
	22.82	22.89	23.18	23.35	20.44	20.44	20.47
	47.80	66.05	111.55	138.40	118.25	89.95	91.20
0.643	2.27	2.30	2.43	2.49	0.00	0.00	0.00
	22.94	23.03	23.42	23.64	20.41	20.38	20.41
	65.55	82.25	123.40	147.75	109.00	75.55	75.85
0.750	2.30	2.33	2.48	0.00	0.00	0.00	0.00
	23.06	23.17	23.61	20.46	20.40	20.35	20.36
	113.35	125.05	154.60	152.05	106.60	63.45	58.40
1.000	2.40	2.45	2.55	0.00	0.00	0.00	0.00
	23.51	23.61	23.90	20.50	20.45	20.37	20.33

TABLE II. Calculated bcc-to-hcp PES for given (η, ϵ) at 10.5 GPa. Legend is the same as in Table I.

ϵ \ η	0.00	0.25	0.50	0.643	0.75	0.95	1.00
	0.00	23.85	83.05	121.55	150.10	199.60	210.75
0.000	2.14	2.14	2.18	2.20	2.20	2.17	2.16
	21.71	21.70	21.89	22.01	22.08	22.16	22.17
	7.95	31.30	88.55	125.10	151.40	110.15	116.30
0.250	2.14	2.14	2.18	2.20	2.20	0.00	0.00
	21.67	21.71	21.87	21.98	22.04	19.92	19.95
	31.65	53.80	108.20	141.55	69.80	48.05	51.45
0.500	2.16	2.16	2.19	2.21	0.00	0.00	0.00
	21.76	21.78	21.91	22.01	19.80	19.80	19.82
	52.90	74.45	126.20	157.10	49.85	21.05	22.75
0.643	2.18	2.18	2.20	2.22	0.00	0.00	0.00
	21.86	21.85	21.98	22.03	19.76	19.77	19.76
	73.10	93.55	142.90	81.05	40.00	5.70	6.35
0.750	2.19	2.20	2.23	0.00	0.00	0.00	0.00
	21.90	21.94	22.04	19.81	19.76	19.72	19.72
	128.70	145.30	170.20	86.45	38.60	−7.25	−9.20
1.000	2.20	2.19	1.13	0.00	0.00	0.00	0.00
	22.07	22.07	20.57	19.85	19.76	19.70	19.69

TABLE III. Calculated bcc-to-hcp PES for given (η, ϵ) at 22 GPa. Legend is the same as in Table I.

ϵ \ η	0.00	0.25	0.50	0.643	0.75	1.00
	0.00	25.70	90.70	108.50	127.10	146.65
0.000	2.06	2.07	2.09	0.00	0.00	0.00
	20.73	20.77	20.90	19.35	19.36	19.45
	1.45	26.60	90.80	103.40	100.75	111.85
0.100	2.06	2.06	2.07	0.00	0.00	0.00
	20.74	20.75	20.86	19.31	19.31	19.41
	8.85	33.25	95.45	88.50	61.95	61.05
0.250	2.07	2.06	2.07	0.00	0.00	0.00
	20.77	20.77	20.87	19.26	19.25	19.31
	35.10	57.95	111.40	44.90	9.50	−8.45
0.500	2.07	2.07	0.00	0.00	0.00	0.00
	20.80	20.82	19.27	19.20	19.17	19.19
	59.05	80.55	100.90	28.65	−11.50	−38.90
0.643	2.08	2.06	0.00	0.00	0.00	0.00
	20.92	20.84	19.27	19.18	19.14	19.14
	81.75	101.85	98.50	21.25	−21.75	−56.45
0.750	2.10	2.05	0.00	0.00	0.00	0.00
	20.94	20.87	19.28	19.18	19.13	19.10
	138.10	145.00	114.30	27.90	−22.55	−73.20
1.000	1.70	1.52	0.00	0.00	0.00	0.00
	20.53	20.28	19.33	19.22	19.15	19.07

[1] R. Jeanloz, Annu. Rev. Earth Planet Sci. **18**, 357 (1990).
[2] D. Bancroft, E. L. Peterson, and S. Minshall, J. Appl. Phys. **27**, 291 (1956).
[3] A. P. Jephcoat, H. K. Mao, and P. M. Bell, J. Geophys. Res. **91**, 4677 (1986).
[4] W. A. Bassett and E. Huang, Science **238**, 780 (1987).
[5] E. Huang, W. A. Bassett, and P. L. Tao, J. Geophys. Res., [Solid Earth Planets] **92**, 8129 (1987).
[6] Q. Williams, R. Jeanloz, Jay Bass, Bob Svendsen, and T. J. Ahrens, Science **236**, 181 (1987).
[7] R. D. Taylor and M. P. Pasternak, J. Appl. Phys. **69**, 6126 (1991).
[8] R. Boehler, Nature (London) **363**, 534 (1993).
[9] S. K. Saxena, G. Shen, and P. Lazor, Science **260**, 1312 (1993).
[10] J. P. Rueff, M. Krisch, Y. Q. Cai, A. Kaprolat, M. Hanfland, M. Lorenzen, C. Masciovecchio, R. Verbeni, and F. Sette, Phys. Rev. B **60**, 14510 (1999).
[11] D. H. Kalantar, J. F. Belak, G. W. Colins *et al.*, Phys. Rev. Lett. **95**, 075502 (2005).
[12] O. Mathon, F. Baudelet, J. P. Itié, A. Polian, M. d'Astuto, J. C. Chervin, and S. Pascarelli, Phys. Rev. Lett. **93**, 255503 (2004).
[13] T. Asada and K. Terakura, Phys. Rev. B **46**, 13599 (1992).
[14] L. Stixrude, R. E. Cohen, and D. J. Singh, Phys. Rev. B **50**, 6442 (1994).
[15] P. Soderlind, J. A. Moriarty, and J. M. Wills, Phys. Rev. B **53**, 14063 (1996).
[16] M. Ekman, B. Sadigh, K. Einarsdotter, and P. Blaha, Phys. Rev. B **58**, 5296 (1998).
[17] K. J. Caspersen, A. Lew, M. Ortiz, and E. A. Carter, Phys. Rev. Lett. **93**, 115501 (2004).
[18] G. Steinle-Neumann, L. Stixrude, and R. E. Cohen, Proc. Natl. Acad. Sci. U.S.A. **101**, 33 (2004).
[19] A. B. Belonoshko, R. Ahuja, and B. Johansson, Nature (London) **424**, 1032 (2003).
[20] A. S. Mikhaylushkin, S. I. Simak, L. Dubrovinsky, N. Dubrovinskaia, B. Johansson, and I. A. Abrikosov, Phys. Rev. Lett. **99**, 165505 (2007).
[21] L. Dubrovinsky *et al.*, Science **316**, 1880 (2007).
[22] W. G. Burgers, Physica **1**, 561 (1934).
[23] K. J. Caspersen and E. A. Carter, Proc. Natl. Acad. Sci. U.S.A. **102**, 6738 (2005).
[24] G. Henkelman and H. Jónsson, J. Chem. Phys. **113**, 9978 (2000).
[25] D. F. Johnson and E. A. Carter, J. Chem. Phys. **128**, 104703 (2008).
[26] P. A. Lindgard and O. G. Mouritsen, Phys. Rev. Lett. **57**, 2458 (1986).
[27] M. Sanati, A. Saxena, T. Lookman, and R. C. Albers, Phys. Rev. B **63**, 224114 (2001).
[28] V. Thakor, J. B. Staunton, J. Poulter, S. Ostanin, B. Ginatempo, and E. Bruno, Phys. Rev. B **67**, 180405(R) (2003).
[29] G. Kresse and J. Furthmuller, Phys. Rev. B **54**, 11169 (1996).
[30] G. Kresse and J. Furthmuller, Comput. Mater. Sci. **6**, 15 (1996).
[31] G. Kresse and D. Joubert, Phys. Rev. B **59**, 1758 (1999).
[32] J. P. Perdew and Y. Wang, Phys. Rev. B **45**, 13244 (1992).
[33] H. J. Monkhorst and J. D. Pack, Phys. Rev. B **13**, 5188 (1976).
[34] B. C. Garrett, M. J. Redmon, R. Steckler, D. G. Truhlar, K. K. Baldridge, D. Bartol, M. W. Schmidt, and M. S. Gordon, J. Phys. Chem. **92**, 1476 (1988).
[35] W. L. Hase and R. J. Duchovic, J. Chem. Phys. **83**, 3448 (1985).
[36] C. Gonzalez and H. B. Schlegel, J. Chem. Phys. **90**, 2154 (1989).
[37] *Mathematica Edition: Version 5.2* (Wolfram Research, Inc., Champaign, IL, 2005).
[38] With $\kappa^2=\Sigma_i(E_i-F_i)/N$, E_i is the DFT energy difference of ith data point, F_i is the value obtained from the fit, and N is the number of the data point.
[39] V. P. Dmitriev, S. B. Rochal, Yu. M. Gufan, and P. Toledano, Phys. Rev. Lett. **60**, 1958 (1988).